

Towards Accurate Force Control of Series Elastic Actuators Exploiting a Robust Transmission Force Observer

Chan Lee¹, Jinhoh Lee², and Sehoon Oh¹

Abstract—This paper develops an accurate force control algorithm for series elastic actuators (SEAs) based on a novel force estimation scheme, called transmission force observer (TFOB). The proposed method is designed to improve an inferior force measurement of the SEA caused by nonlinearities of the elastic transmission and measurement noise and error of its deformation sensor. This paper first analyzes the limitation of the conventional methods for the SEA transmission force sensing and then investigates its stochastic characteristics, which indeed provide the base to render the accurate force control performance incorporated with the TFOB. In particular, a tuning parameter is introduced from holistic closed-loop system analyses in the frequency domain. This gives a guideline to attain optimum performance of the force-controlled SEA system. The proposed algorithm is experimentally verified in an actual SEA hardware setup.

I. INTRODUCTION

A highly accurate force control of an actuator is a core technology for the modern mechatronic systems, robotics, and industrial applications which enables dynamic control with high fidelity allowing not only rapid tracking performance but also compliant behavior. In particular, a collaborative robot, which is one of key drivers in recent technologies such as Industry 4.0, essentially requires the precise force control capability in its actuation. This has also promoted the development of force sensing methods such as sensor-based measurement or sensorless estimation in the force-controlled actuator system.

Series elastic actuators (SEAs) have facilitated the aforementioned applications owing to its inherent capability to control output force without an extra force sensor or estimation algorithms [1]. The SEA employs an elastic element instead of a stiff mechanical structure of the force sensor and the intrinsic compliance leads to both superior force control and safe interaction, where the force measurement can be acquired through strain-stress phenomenon. Accordingly, the precision and the robustness of force control in the SEA system become highlighted as an essential issue [2] aiming at not only high force fidelity, but also dynamic motion with compliant behaviors in high-level robot control applications [3], [4].

¹The authors are with Department of Robotics Engineering, Daegu Gyeongbuk Institute of Science and Technology(DGIST), Daegu, Korea, 711-785. ²Jinhoh Lee is with Department of Advanced Robotics, Istituto Italiano di Tecnologia (IIT), Via Morego 30, 16163, Genova, Italy. (Chan Lee and Jinhoh Lee are co-first authors.)

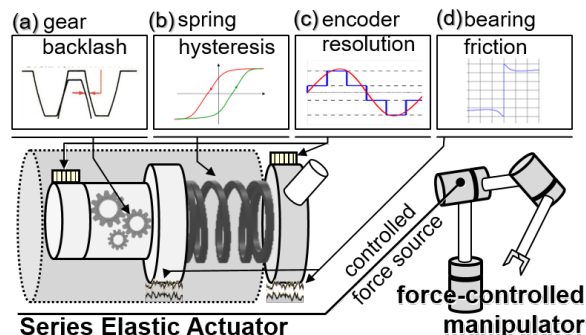


Fig. 1. The sources of inaccuracy in the force measurement and control of SEAs: (a) the gear transmission such as a backlash, (b) mechanical behavior of the spring, (c) errors in encoder measurement signals, and (d) the frictions.

For the force-controlled SEA, the force in the elastic transmission is generally given by the assumption that the transmission force can be simply calculated from a linear spring model and its deflection measured by encoders [5]. Ideally, the SEA with this deflection-based transmission force sensing can offer better force control performance than that with the load cell type measurement. However, it suffers from considerable inaccuracy caused by the inherent nonlinearities in the components in the SEA such as backlash and friction effect in a gear train and the hysteresis in strain-stress characteristics of the spring element, as illustrated in Fig. 1. It is also known that the low resolution of the encoders and noises in the deflection measurement result in performance degradation.

To mitigate these issues, significant efforts have been made in two folds: 1) control design approaches and 2) observer design approaches. First, in the control design-oriented approaches, a common remedy is to compensate the measurement inaccuracy by using a lookup table between the encoder measurement of SEA and the force measured by a load cell as its ground truth [6]. This approach can be applied in a practical way when the measurement errors are deterministic in the operating positions of the SEA. Wang et al. [7] and Choi et al. [8] have analyzed the hysteresis effect of the spring in the SEA, and have proposed compensation methods based on hysteresis models. On the other hand, this problem was also tackled by applying robust controllers. Makarov et al. proposed an H_∞ control method for the elastic joint robot with uncertainties [9]. In [2], Oh and Kong developed a disturbance observer (DOB)-based controller for SEAs which can reject the external (load side) and the internal (spring and motor

sides) disturbances.

Second, there have been model-based observer approaches to fundamentally enhance the SEA sensing capability for better force control. Austin et al. adopted a Luenberger observer for state estimation of the SEA equipped with the nonlinear rubber spring [10]. Extending this idea benefiting from the use of SEA dynamics to overcome the measurement issues, some research groups have exploited the motor-side dynamic model and measurement as an alternative to the spring deformation-based force measurement. This method has been implemented in forms of the residual-based observer [11], [12] and the disturbance observer [13], and further improved by using both motor side dynamics and spring information [14], [15].

Interestingly, it is noted that the research has been rarely conducted to incorporate the force controller and the model-based observer for the SEA, in spite of potential advantages expected from both approaches. One example is the sliding mode control method for the position control of an elastic joint, proposed in [16], which utilized the residual-based force observer using motor-side dynamics to overcome hysteresis and friction effects. Although the model-based observer is successfully combined with the position controller of the elastic joint, it is difficult to extend the control methodology directly to the SEA force control. Hence, designing force control with transmission force estimation techniques is still challenging, yet worthwhile to attain accurate and robust performance in SEAs.

This paper thus aims to develop an SEA force controller with high precision taking full advantage of a robust force estimation method to overcome defective force measurement. The proposed algorithm is designed through analyses of the measurement error characteristics of the SEA, and quantitatively optimized with the consideration of the dynamics, the controller and the observer of the entire closed-loop system.

The rest of the paper is organized as follows: first, the errors in the SEA force measurement and their characteristics are mathematically modeled and analyzed in Section II. Section III presents the design and verification of a novel force observer for SEAs, named transmission force observer (TFOB). With exploitation of the TFOB, a force control algorithm is proposed in Section IV. Particularly, a systematic tuning method to obtain the accurate and robust force control performance is given based on the insight from error analyses. Section V experimentally verifies the holistic force control algorithm with TFOB in the real SEA test bench.

II. PROBLEMS IN FORCE MEASUREMENT OF SEAS

To deal with the accurate force estimation/control problem, inaccuracy issues of the conventional deformation-based force measurement in SEA are analyzed in this section. Firstly, the mathematical model for deformation-based force measurement is defined to confirm error factors which are discussed in this paper. In order to explore the behavior of the errors, two types of experimental analyses are conducted. One is deterministic analysis, and the second is stochastic analysis. The deterministic analysis verifies the non-linear characteristic of deformation-based force measurement, and stochastic

analysis indicates that the nonlinear characteristic of the SEA force measurement error is regarded as Gaussian noise. The Gaussian characteristic of the error will provide a connection to the performance optimization of the force controller design in Section IV.

A. Errors in Deformation-based Force Measurement

Conventional force/torque measurement of SEA, called deformation-based force measurement (DFM), is usually given as follows:

$$\hat{\tau}_s^s = K_s^n \theta_s^m, \quad (1)$$

where $\hat{\tau}_s^s$ is the estimated spring force, K_s^n is the nominal spring stiffness, and θ_s^m is the measured spring deformation by encoders. Note that the term ‘force’ is used for general explanations hereinafter, while the term ‘torque’ is used for one regarding the experimental results since a rotary-type SEA is set as the experiment hardware.

However, in this DFM, the accuracy is often deteriorated because $\hat{\tau}_s^s$ is subject to error factors such as encoder resolution, noise, backlash in gears and uncertainty in spring behavior as depicted in Fig. 1. These defective factors can be categorized as two folds: θ_s^e , the error of deformation measurement itself (resolution and noise problem), and K_s^e , the errors in estimation model (spring hysteresis, friction and backlash).

The DFM (1) can be rewritten with consideration of the error factors K_s^e and θ_s^e as

$$\begin{aligned} \hat{\tau}_s^s &= (K_s + K_s^e)(\theta_s + \theta_s^e), \\ &= K_s \theta_s + K_s^e \theta_s + K_s \theta_s^e + K_s^e \theta_s^e, \end{aligned} \quad (2)$$

where $K_s \theta_s$ is actual force exerting from the spring, and the terms $K_s^e \theta_s$, $K_s \theta_s^e$ and $K_s^e \theta_s^e$ represent errors. The errors in (2) can be rearranged as follows:

$$\begin{aligned} \hat{\tau}_s^s &= \tau_s + K_s \left(\frac{K_s^e}{K_s} \theta_s + \frac{K_s^n}{K_s} \theta_s^e \right), \\ &= \tau_s + K_s (\xi_s^m + \xi_s^e), \\ &= \tau_s + K_s \xi_s^*, \end{aligned} \quad (3)$$

where ξ_s^* is a total measurement error including mechanical error ξ_s^m and encoder measurement error ξ_s^e . The influence of ξ_s^* on the force measurement $\hat{\tau}_s^s$ changes depending on the level of K_s^n ; the larger the spring stiffness is, the more affected by the measurement noise the force measurement is.

To further investigate this problem, we perform force measurement experiments, where the torque output of the rotary-type SEA was measured based on DFM in (1) and compared with the torque reading from an additional torque sensor equipped as the ground truth. (Refer to the details of the experimental setup in Section V-A.) Fig. 2(a) shows the result of comparison between the DFM of SEA and actual torque. One can clearly observe the discrepancy between the DFM and ground-truth torque, while their trends are well-matched. This discloses two issues: 1) the offset of 2 Nm (in particular, when the direction of the force changes), mainly due to the hysteresis of the spring or the backlash among gears; and 2) the noises. The former error corresponds to ξ_s^m , which is caused by the mechanism, while the latter error corresponds to ξ_s^e .

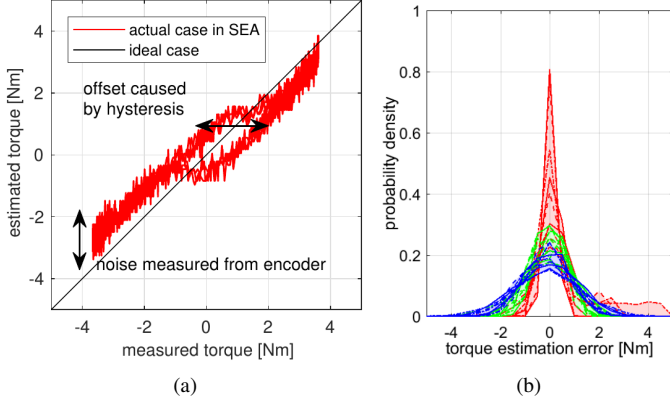


Fig. 2. Plots of torque estimation errors caused by nonlinear characteristics: (a) experimental analyses of deterministic behavior and (b) stochastic behavior, where blue, green and red colors indicate high (9100 Nm/rad), mid (2500 Nm/rad) and low (60 Nm/rad) stiffness values.

B. Stochastic Characteristics of the Measurement Errors

The measurement error ξ_s^* of DFM exhibits stochastic characteristics, which can be apparently verified with measurement experiments under regulated pattern torque generation. For analysis of this characteristic, experiments have been conducted, where the SEA is controlled to generate several sinusoidal pattern torque outputs.

In the experiment, a torque sensor is connected between an SEA and a fixed environment to measure the accurate torque output of SEA. For in-depth analysis of the measurement error under various operating condition, 9 types of sinusoidal torque references (3 different frequencies \times 3 different magnitudes) and three types of spring settings (low, mid and high stiffness) were tested in the experiments. In each experiment, the torque outputs of SEA were estimated by DFM (1) and compared with the torque sensor measurements. The difference between two was calculated, and Fig. 2(b) illustrates the distribution of these differences, which are the estimation error by DFM.

From the error distributions, one can notice that the torque error measurement of SEA is regarded to have Gaussian distribution. The comparison among three different spring stiffness verifies that large spring stiffness K_s leads to large torque estimation error.

It is well known that the encoder quantization error can be modeled as Gaussian noise, and the result verifies that the torque estimation is affected by this Gaussian encoder noise. This implies that the low resolution encoder with high stiffness spring can lead to very inaccurate force estimation.

This observation shows that the DFM error factor ξ_s^* can be considered Gaussian, the magnitude of which can be evaluated using the variance. This point can be utilized in the feedback controller design to quantitatively evaluate controllers.

III. ROBUST TRANSMISSION FORCE OBSERVER (TFOB)

A. Design of the TFOB

In this section, an observer to estimate the SEA force output is proposed to address this inaccurate force estimation. The observer exploits the fact that the SEA output force works as the external disturbance (reacted spring force) with respect

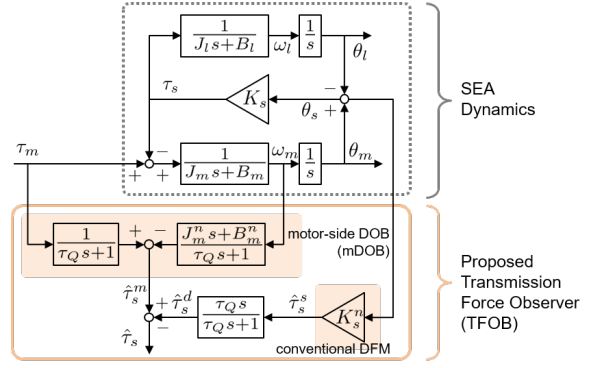


Fig. 3. Block diagram of the proposed TFOB for SEAs.

to the motor dynamics, which allows for utilization of force observer concept [17]–[19] to observe the SEA output force as the external disturbance.

Fig. 3 shows the dynamics of SEA with the force observer design; the SEA dynamics in the upper block diagrams consists of the motor dynamics $P_m(s) = \frac{1}{J_m s + B_m}$, the spring K_s and the load dynamics $P_l(s) = \frac{1}{J_l s + B_l}$, where J_\bullet and B_\bullet represent inertia and damping values of motor-and load-sides. The output force of SEA is presented as $K_s \theta_s$.

A motor-side DOB (mDOB) of SEA is designed by utilizing the nominal motor dynamics $P_m^n(s) = \frac{1}{J_m^n s + B_m^n}$, which can estimate the external force at the motor-side. In this case, the spring force $K_s \theta_s$ corresponds to the external force.

The estimate of the spring force by mDOB can be formulated as follows:

$$\hat{\tau}_s^m = -Q(s) \left(P_m^{n-1}(s) \omega_m^m - \tau_m \right), \quad (4)$$

where $Q(s)$ denotes the Q filter expressed as a form of the low-pass filter— $Q(s) = \frac{1}{\tau_Q s + 1}$ in this paper, and ω_m^m denotes the motor angular velocity measured as follows:

$$\omega_m^m = s(\theta_m + \xi_m^*), \quad (5)$$

where ξ_m^* represents the measurement error of the motor encoder caused by mechanical quantization or noise, and thus ω_m^m is influenced by numerical differentiation of measurement errors. Note that the Q filter $Q(s)$ should be added to reduce this error, whereas it also limits the estimation performance only within the bandwidth of $Q(s)$, where the cut-off frequency is denoted as $\omega_Q = 1/\tau_Q$.

Accordingly, the spring force can be estimated in two ways: $\hat{\tau}_s^s$ by DFM as in (1) and $\hat{\tau}_s^m$ by the above mDOB. Each estimate has its own drawback: τ_s^s has offset and noise problem and τ_s^m has bandwidth limitation.

To overcome these drawbacks, this paper proposes a novel algorithm to integrate two estimates in a complementary way. The integrated transmission force observer (TFOB) to achieve accurate force estimation is designed as follows.

$$\begin{aligned} \hat{\tau}_s &= \hat{\tau}_s^m + (1 - Q(s))\hat{\tau}_s^s = \hat{\tau}_s^m + \hat{\tau}_s^d \\ &= Q(s) \left(\tau_m - P_m^{n-1}(s) \omega_m^m \right) + (1 - Q(s)) K_s^n \theta_s^m \\ &= \tau_s + \left(Q(s) P_m^{n-1}(s) s \xi_m^* - (1 - Q(s)) K_s^n \xi_s^* \right) \end{aligned} \quad (6)$$

TABLE I
RMS ERRORS OF SPRING FORCE ESTIMATION METHODS

ω_Q	(a) 0.1 Hz	(b) 1 Hz	(c) 5 Hz	(d) 10 Hz
TFOB-based	0.678 Nm	0.311 Nm	0.298 Nm	0.403 Nm
DFM-based	0.770 Nm	0.791 Nm	0.783 Nm	0.817 Nm

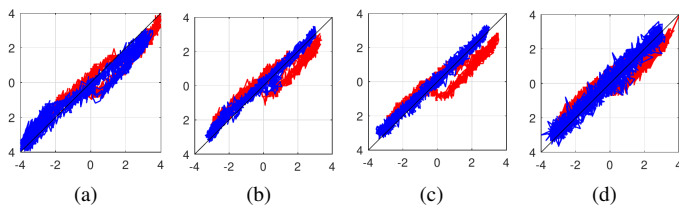


Fig. 4. TFOB performances with regards to varying Q filter bandwidth, ω_Q : (a) 0.1 Hz, (b) 1 Hz, (c) 5 Hz, and (d) 10 Hz. Red and blue lines indicate the results of DFM and TFOB respectively. x -axis is the estimated torque, and y -axis is the measured torque [Nm].

The conventional force estimation τ_s^s is high pass-filtered in the proposed TFOB as shown in (6). The offset issue in τ_s^s can be addressed by this high pass filtering. The cut-off frequency of $Q(s)$ is the tuning factor of TFOB, which determines the bandwidths of mDOB-based estimation and high pass-filtered DFM. Note that the baseline of TFOB is inspired from [20], however, it is redesigned in a different form with consideration of the motor-side encoder noise to extend the analysis to a controller optimization problem in Section IV.

B. Verification of Estimation Accuracy of Proposed TFOB

In order to verify the performance of TFOB, the estimation experiments were performed, and the results were compared with the torque sensor measurement. In particular, the experiments were conducted using various Q filter bandwidth settings of TFOB, in search of the optimal bandwidth value. This will give a notion that the Q filter bandwidth can be further exploited to achieve optimal force control performance (discussed in Section IV).

Fig. 4 shows results of the estimation by TFOB compared with conventional DFM estimate. In the experiments, the bandwidths of Q filters ω_Q varies from (a) 0.1 Hz to (d) 10 Hz. In all subplots in Fig. 4, the red lines indicate results of DFM, and the blue lines indicate results of TFOB.

DFM results show large off-sets up to 1 Nm, even though it exhibits good linearity. In contrast, TFOB can successfully reduce the error in all the results. Comparison of (a) to (c) reveals that high ω_Q can reduce the error more effectively. However, when the bandwidth of the TFOB increases to 10 Hz, the noise increases in the estimate and shows worse estimation result than 5 Hz. This is due to error in the measurement of the motor-side encoder, ξ_m^* .

In order to quantitatively show these trade-off characteristics, the Root Mean Square Error (RMSE) values of the estimation are compared in Table I. The result shows that the TFOB with 5 Hz bandwidth shows the best performance.

IV. ACCURATE FORCE CONTROL BASED ON TFOB

In this section, design method of force controllers utilizing TFOB is proposed, and its characteristic is analyzed in terms of accuracy or robustness against measurement errors. Finally,

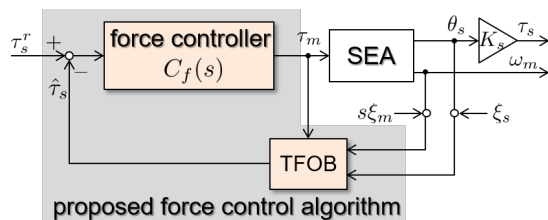


Fig. 5. The block diagram of the proposed force control with the TFOB.

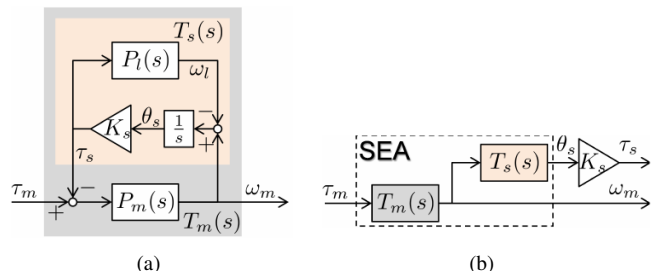


Fig. 6. Block diagram of the dynamic model of the SEA.

a methodology to tune Q filter of TFOB is discussed taking into consideration the dynamic characteristics of TFOB-based force control.

A. Design of TFOB-based Force Controller

TFOB does not conform the force controller of SEA, in other words, any type of controller that has been proposed for high performance control of SEA force output can benefit from the TFOB by replacing the conventional force estimate $\hat{\tau}_s^s$ with the TFOB output $\hat{\tau}_s$. The control law of the proposed TFOB-based force control is designed as

$$\begin{aligned} \tau_m &= C_f(s) (\tau_s^r - \hat{\tau}_s), \\ &= C_f(s) \{ \tau_s^r - Q(s) (\tau_m - P_m^{-1}(s)\omega_m) \\ &\quad - (1 - Q(s)) K_s \theta_s \}. \end{aligned} \quad (7)$$

Fig. 5 illustrates the proposed control configuration utilizing feedback from the TFOB output, where the force controller $C_f(s)$ can be designed as any types of controllers, e.g., proportional-integral-derivative (PID) control, DOB, or sliding-mode control.

In this paper, the conventional PD controller is employed for the force controller $C_f(s)$, as it is the most general and widely-utilized control design methodology. In the following subsections, two aspects are to be examined: 1) how the TFOB can improve the force control performance and 2) how to tune the Q filter when a controller is given.

B. Open-loop Analysis of SEA Dynamics

To design and analyze TFOB-based force controller, the dynamics of SEA is investigated at first. Fig. 6 re-illustrates the block diagram of an SEA in Fig. 3 with the motor $P_m(s)$, the spring K_s and the load $P_l(s)$ dynamics.

As two outputs, $\theta_s (\propto \tau_s)$ and ω_m are utilized for TFOB, the transfer function from the motor torque τ_m to these two outputs need to be derived as follows:

$$\frac{\theta_s}{\tau_m} = \frac{P_m(s)}{s + K_s(P_m(s) + P_l(s))} \quad (8)$$

$$\frac{\omega_m}{\tau_m} = \frac{P_m(s)(s + K_s P_l(s))}{s + K_s(P_m(s) + P_l(s))} = T_m(s). \quad (9)$$

From these transfer functions, the relationship between two outputs θ_s and ω_m is derived as

$$\theta_s = \frac{1}{s + K_s P_l(s)} \omega_m = T_s(s) \omega_m. \quad (10)$$

From the viewpoint of motor dynamics $P_m(s)$, $\tau_s = K_s T_s(s) \omega_m$ is considered external force, which forms a feedback loop through $P_m(s) T_s(s) K_s$. This relationship finalizes the transfer function from the motor torque to the motor angular velocity re-organized using $T_s(s)$ as

$$\frac{\omega_m}{\tau_m} = T_m(s) = \frac{P_m(s)}{1 + K_s P_m(s) T_s(s)}. \quad (11)$$

In the same way, the transfer function to the force output of SEA τ_s is derived as

$$\frac{\tau_s}{\tau_m} = K_s T_s(s) T_m(s) = \frac{K_s P_m(s) T_s(s)}{1 + K_s P_m(s) T_s(s)}. \quad (12)$$

These transfer functions are utilized for synthesis and analysis of controller in the following subsection.

C. Closed-loop Analysis of TFOB-based Force Control

The reference tracking performance of the proposed control in Fig. 5 is analyzed using the transfer function from the reference τ_s^r to the output τ_s , which is given as follows:

$$\frac{\tau_s}{\tau_s^r} = P_{cl} = \frac{C_f K_s P_m T_s}{1 + (1 + C_f) K_s P_m T_s} \quad (13)$$

Note that the transfer function (13) is the same as that of the conventional DFM-based force control. In other words, the TFOB does not affect the reference tracking characteristic, i.e., the force controller $C_f(s)$ can be designed independently from TFOB. For simplicity of description, hereinafter, the Laplace domain operator (s) of the system is omitted.

The impacts on the control performance from the encoder measurement error ξ_s^e and mechanical modeling error ξ_m^m —collectively expressed as ξ_s given in (3)— can be reduced by TFOB. It can be investigated by the transfer functions from ξ_m and ξ_s to τ_s as follows:

$$\frac{\tau_s}{\xi_s} = (1 - Q) K_s P_{cl}, \quad (14)$$

$$\frac{\tau_s}{\xi_m} = s Q P_m^{-1} P_{cl}. \quad (15)$$

Whereas, the impact of ξ_s on τ_s in the DFM-based force control is given as

$$\frac{\tau_s}{\xi_s} = K_s P_{cl}. \quad (16)$$

As illustrated in Fig. 7, it then can be noticed in the TFOB-based control that the effect of ξ_s is high-pass filtered by $(1 - Q)$ as shown in (14). Besides, ξ_m has no effect on the conventional DFM-based control, but affects τ_s in TFOB-based control which is low-pass filtered by Q shown in (15).

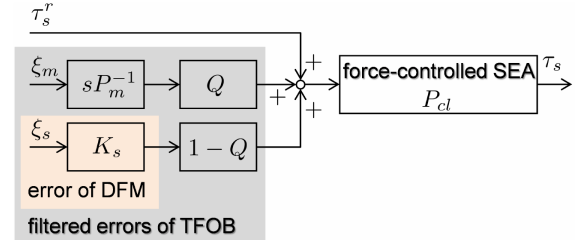


Fig. 7. Influences of errors in the closed-loop of DFM- and TFOB-based force control.

Accordingly, for TFOB-based force control to achieve better error reduction, magnitudes of the transfer functions (14), (15) should be smaller than that of (16). Henceforth, the output force caused by the measurement errors under the TFOB-based control is investigated with various conditions and compared with the DFM-based control.

To handle the error characteristics of two different encoder measurements (ξ_s and ξ_m) in a comprehensive way, two error characteristics are quantified as follows:

$$|\xi_m|^2 = H^2 |\xi_s|^2, \quad (17)$$

which means the ratio of two error magnitudes can be related using arbitrary gain H . In other words, the difference between measurement error conditions of two angles θ_m and θ_s is described by H . For example, if the error is considered due to the encoder quantization, H represents the ratio of the encoder resolutions between the spring encoder and the motor encoder. It is noticeable that the consideration of gear ratio which is necessary when the motor-side encoder is placed before the gear transmission of SEA, can be reflected in H , too.

With the relationship in (17), the effects of the measurement error on the SEA force output under the TFOB-based control can be calculated as

$$\tau_s^e = \frac{C_f(1 - Q)P_m K_s^2 T_s \xi_s + s C_f Q K_s T_s \xi_m}{1 + K_s P_m T_s \{1 + C_f\}}, \quad (18)$$

and its norm (magnitude) is given as

$$\begin{aligned} \|\tau_s^e\| &= \left\| \frac{C_f(1 - Q)P_m K_s^2 T_s \xi_s + s C_f Q K_s T_s \xi_m}{1 + K_s P_m T_s \{1 + C_f\}} \right\| \\ &\leq \left\| \frac{C_f(1 - Q)P_m K_s^2 T_s}{1 + K_s P_m T_s \{1 + C_f\}} \right\| \|\xi_s\| + \\ &\quad \left\| \frac{s C_f Q K_s T_s}{1 + K_s P_m T_s \{1 + C_f\}} \right\| \|\xi_m\| \\ &= \left(\left\| \frac{C_f(1 - Q)P_m K_s^2 T_s}{1 + K_s P_m T_s \{1 + C_d\}} \right\| + \right. \\ &\quad \left. \left\| \frac{s H C_f Q K_s T_s}{1 + K_s P_m T_s \{1 + C_f\}} \right\| \right) \|\xi_s\| = \|\tau_s^{TFOB}\|. \end{aligned} \quad (19)$$

Meanwhile, the same error characteristic with the conventional DFM-based control is given as

$$\|\tau_s^{DFM}\| = \left\| \frac{C_f P_m K_s^2 T_s}{1 + K_s P_m T_s \{1 + C_f\}} \right\| \|\xi_s\|. \quad (20)$$

By comparing the magnitude of (19) and (20), the effects of the measurement errors on the output force with the proposed

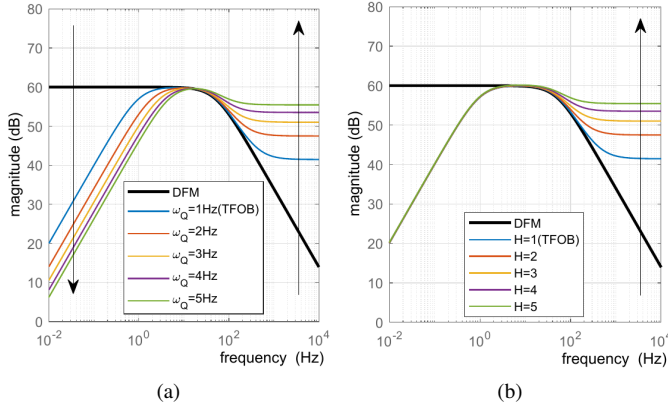


Fig. 8. Influences of measurement errors in SEA force output according to (a) Q filter bandwidth of TFOB, (b) motor encoder performance (higher H means low quality encoder.)

TFOB feedback control and DFM feedback control can be derived and compared.

In Fig. 8, the magnitudes with TFOB feedback in (19) are calculated with different Q filter bandwidths and H values. As seen in the plots, the magnitude with the TFOB-based control is lower than that with the DFM-based control in the low frequency range, while it becomes higher in the high frequency range. In details, Fig. 8(a) shows that Q filter bandwidth can change the reduction of the magnitude in the low frequency range, while it will sacrifice the high frequency magnitudes. Moreover, it is interesting that H in Fig. 8(b), the error characteristic of the motor side encoder does not change the low frequency magnitude of the TFOB-based control. Namely, TFOB-based control improves the low frequency error characteristic regardless of motor encoder resolution. But in the high frequency range, the error characteristic is deteriorated as H increases.

This analysis verifies that the bandwidth frequency of the TFOB Q filter is a tuning factor that adjusts the trade-off between two errors ξ_m and ξ_s . The bandwidth of error attenuation can be improved by Q filter bandwidth at the sacrifice of the high frequency error magnitude, which is determined by the characteristic of the motor-side encoder.

D. Tuning method for TFOB-based Control

Our ultimate goal is to find optimal Q filter bandwidth ω_Q under the TFOB-based force control, where the condition can be described as follows:

$$\|\tau_s^{TFOB}\| < \|\tau_s^{DFM}\| \quad (21)$$

For the TFOB-based control to achieve better error reduction performance than the conventional DFM-based force control as described in (21), the magnitude of (19) should be less than (20) as follows:

$$\underbrace{\left\| \frac{C_f(1-Q)P_mK_s^2T_s}{1+K_sP_mT_s(1+C_f)} \right\|}_{\text{error characteristics of TFOB-based control in (19)}} + \left\| \frac{sHC_fQK_sT_s}{1+K_sP_mT_s(1+C_f)} \right\| < \underbrace{\left\| \frac{C_fP_mK_s^2T_s}{1+K_sP_mT_s(1+C_f)} \right\|}_{\text{error characteristics of DFM-based control in (20)}} \quad (22)$$

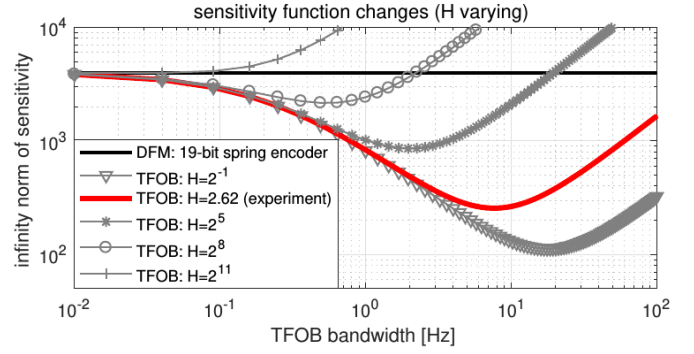


Fig. 9. Comparison of sensitivity against measurement error with TFOB.

It is difficult to find Q filter condition to satisfying (22) in all frequency ranges, however, the condition to set the infinity norm of two transfer functions as in (23) can be found as

$$\left\| \frac{C_f(1-Q)P_mK_s^2T_s}{1+K_sP_mT_s(1+C_f)} \right\|_{\infty} + \left\| \frac{sC_fQK_sT_sH}{1+K_sP_mT_s(1+C_f)} \right\|_{\infty} < \left\| \frac{C_fP_mK_s^2T_s}{1+K_sP_mT_s(1+C_f)} \right\|_{\infty} \quad (23)$$

With the Q filter design in (23), the maximum force output error of TFOB-based control is guaranteed to be less than that of DFM-based control as follows [21]:

$$\max_{\xi_s(t)} \frac{\|\tau_s^{TFOB}(t)\|_2}{\|\xi_s(t)\|_2} < \max_{\xi_s(t)} \frac{\|\tau_s^{DFM}(t)\|_2}{\|\xi_s(t)\|_2} \quad (24)$$

This induced norm relationship satisfies the optimization goal in (21), thus, the problem in (21) can be reconsidered as a finding of Q filter bandwidth ω_Q which satisfies the condition in (23). For brevity, the condition (23) can be re-arranged as

$$\|(1-Q)K_s\|_{\infty} + \|sQHP_m^{-1}\|_{\infty} < \|K_s\|_{\infty} \quad (25)$$

Fig. 9 shows the comparison of two infinity norms $\|(1-Q)K_s\|_{\infty} + \|sQHP_m^{-1}\|_{\infty}$ and $\|K_s\|_{\infty}$ in (25) with regard to the bandwidth of Q filter in the x -axis to examine how the measurement error condition changes the magnitude. The parameters, required for the comparison, are from Table II, which is same as the experimental setup in Fig. 10. The black thick solid line represents $\|K_s\|_{\infty}$ which corresponds to the infinity norm of the DFM-based control sensitivity function in (20), and other marked lines represent $\|(1-Q)K_s\|_{\infty} + \|sQHP_m^{-1}\|_{\infty}$ which corresponds to the infinity norm of the TFOB-based control sensitivity function in (19). Various H levels are also considered in Fig. 9, from 2^{-1} to 2^{11} .

Interestingly, the comparative result indicates that there is an optimal frequency bandwidth which minimizes $\|(1-Q)K_s\|_{\infty} + \|sQHP_m^{-1}\|_{\infty}$ such that TFOB-based control achieves the best performance. The effect of H on the performance also can be analyzed using Fig. 9; the smaller H is, the better performance TFOB-based control can achieve; the bandwidth of TFOB value can be set higher when the motor-side encoder exhibits better measurement characteristic so that the performance of TFOB-based control can be improved.

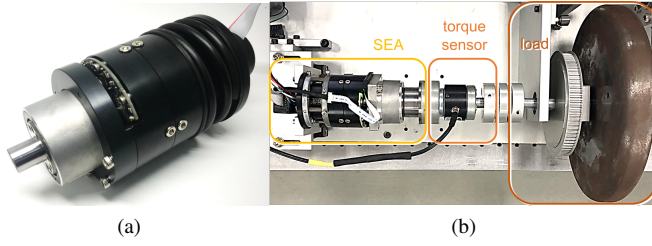


Fig. 10. Experimental setup: (a) the SEA (detailed in [22]), and (b) test bench for SEA torque control and estimation performance verification.

TABLE II
PHYSICAL PARAMETERS OF THE SEA IN THE EXPERIMENT SETUP

notation	parameter	value	unit
J_m	motor inertia	0.0000625	kgm ²
B_m	motor damping	0.0001023	Nms/rad
J_l	load inertia	0.216	kgm ²
J_l	load damping	0.0005	Nms/rad
K_s	spring stiffness	4950	Nm/rad
N	gear ratio	100	-
K_p	proportional gain	1	-
K_d	derivative gain	0.014	-
ω_Q	bandwidth of Q(s)	from 0.1-10	Hz
ξ_m	motor encoder resolution	2000 (x4)	CPT
ξ_s	spring encoder resolution	19	bit
H	error ratio	2.621	-

As explained above, one simple interpretation of H is the ratio of resolutions of two encoders taking the gear ratio also into consideration. With this interpretation, H value of the experimental set up in Fig. 10 is calculated as follows:

$$H = \frac{(\text{resolution of the motor encoder}) \times (\text{gear ratio})}{(\text{resolution of the spring encoder})} = 2.62.$$

The case with $H = 2.62$ is depicted in Fig. 10 (red thick line), where the optimal bandwidth is around from 5-10 Hz, which is to be verified in the following experiment.

V. EXPERIMENTAL VERIFICATION

The performance of the proposed TFOB-based force controller is verified through experiments in this section. At first, the experimental set up equipped with the SEA is introduced, then the following points are experimentally investigated:

- 1) tracking performance of the TFOB-based force control,
- 2) force estimation accuracy during the control,
- 3) robustness against noise coming from the sensor, and
- 4) performance change with bandwidths of the Q filter.

These performance and robustness of the proposed TFOB-based force control are compared with the conventional DFM-based control both in the time domain and the frequency domain.

A. Experimental Setup

1) *Hardware Description*: Fig. 10 illustrates the experimental setup consisting of the rotary type SEA (Fig. 10(a)), the load and the torque sensor. The torque sensor (TNT-200 from Transducer Techniques with 22.6 Nm capacity) can directly measure the SEA torque output transmitted to the load.

Compact Planetary-gearred Elastic Actuator (cPEA) is utilized in this experiment, the detailed structure and operating principle of which are presented in [22]. The physical parameters of the SEA are shown in Table II.

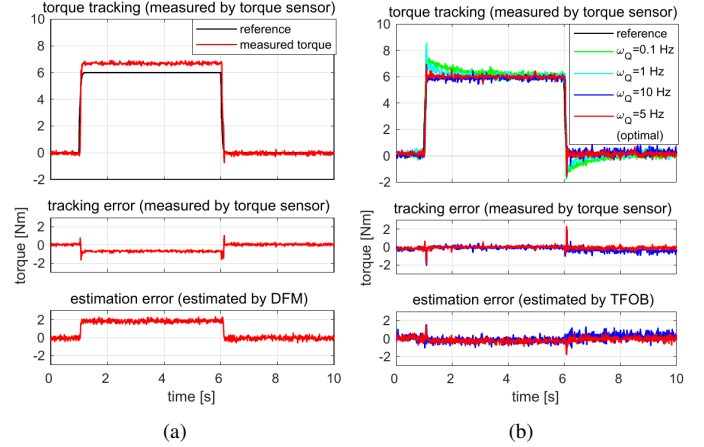


Fig. 11. Time domain reference tracking results of (a) DFM- and (b) TFOB-based force control.

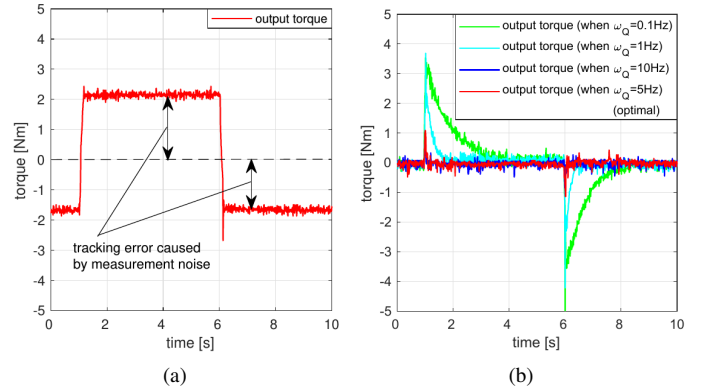


Fig. 12. Spring deflection measurement error rejection results of (a) DFM- and (b) TFOB-based control.

2) *Experimental Protocol*: A proportional-derivative (PD) controller is adopted as the common feedback controller $C_f(s)$ for both DFB- and TFOB-based force control. The performances of two approaches are compared in three ways; 1) reference tracking error comparison with a step-wise reference, 2) deformation measurement error (noise) rejection performance comparison and 3) reference tracking performance comparison with various sinusoidal reference signals. Moreover, various Q filter bandwidths are tested for the TFOB-based force control experiments.

B. Time Domain Experimental Results

1) *Reference Tracking Performance*: A step signal is applied as the reference for both DFM- and TFOB-based force control. The tracking performance is evaluated by the difference between this reference and the actual SEA output torque, measured by a torque sensor.

Fig. 11 shows the results of reference tracking, where 6 Nm step-wise reference is given from 1 s to 6 s; Fig. 11(a) is the result of DFM-based control, and Fig. 11(b) is the results of TFOB-based controls. The output of the DFM-based control case shown in Fig. 11(a) exhibits steady state error which is more than 0.6 Nm (10% of the reference).

On the contrary, TFOB-based force control case in Fig. 11(b) shows no steady state error regardless of how the

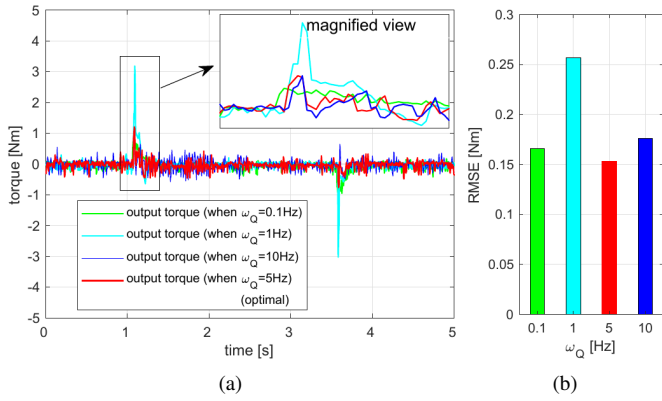


Fig. 13. Motor position measurement error rejection performance TFOB-based control: (a) time domain results and (b) RMSE values.

reference signal changes. Further investigation with different bandwidth of Q filter verifies that higher ω_Q (5 Hz in this case) improves the tracking performance reducing overshoots.

2) *Noise Rejection Performance*: To verify the robustness against measurement errors, an additional step-wise measurement noise (ξ_s^{step} , ξ_m^{step}) is added to the actual measurements θ_m of motor angle and spring deformation θ_s , and the control performance is examined under the noise to investigate the robustness of each controller against this measurement error.

Fig. 12 shows the actual output torque, which is supposed to be kept 0 by DFM-based control (Fig. 12(a)) or TFOB-based control (Fig. 12(b)) with 0 reference. A step-wise measurement error ξ_s^{step} of 0.0005 rad is added to the spring measurement θ_s from 1 s to 5 s. The DFM-based control result in Fig. 12(a) shows that the torque output is significantly affected by the noise, while the TFOB-based control in Fig. 12(b) shows little error against the noise. The attenuation of the torque error against the measurement error depends on the ω_Q , and Fig. 12(b) verifies that the higher ω_Q rejects the effect of the measurement noise better.

Fig. 13(a) illustrates regulation performance of TFOB-based control in time domain when a step-wise error ξ_m^{step} is added to the motor angle measurement θ_m . Even though the measured torque output is affected by the noise, it is shown that higher ω_Q can remove the effect of the noise effectively. However, too high ω_Q (10 Hz, in this experiments) induces chattering in the output, which deteriorates the control performance of SEA. RMSEs are calculated to compare the performances with different ω_Q , and displayed in Fig 13(b). The RMSE comparison in Fig 13(b) shows that $\omega_Q=5$ Hz shows the best regulation performance.

C. Tracking Performance in the Frequency Domain

In this experiment, sinusoidal signals with various frequencies are added to the SEA torque control as the reference, and the RMSE values are calculated for each frequency. The tracking performance in the frequency domain is calculated in this way, and the results with DFM- and TFOB-based control with 4 different ω_Q setting are compared.

Fig. 14 shows the result where each dot represents the RMSE at each frequency (the magnitude of the sinusoidal reference is set to 3 Nm). The tracking errors are compared

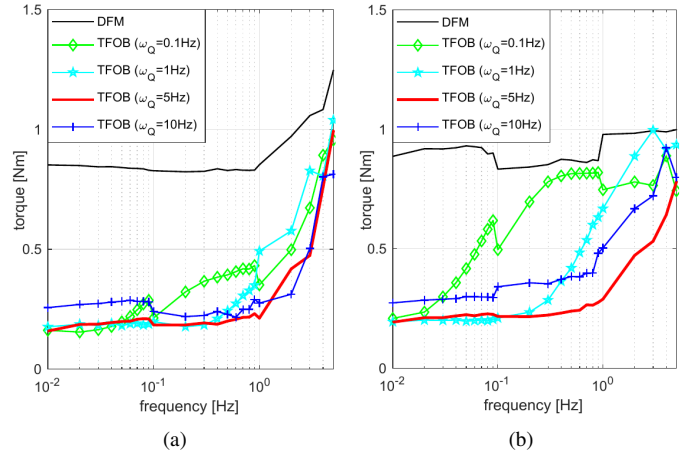


Fig. 14. Frequency domain results of (a) tracking errors and (b) estimation errors under the DFM- and TFOB-based control.

in Fig. 14(a), and the estimation errors are compared in Fig. 14(b), and the results validate that the proposed TFOB-based control can improve the performance compared with the DFM-based control at all frequencies.

VI. CONCLUSION

This paper proposed the accurate force control algorithm for SEA systems based on the TFOB. The contributions of this paper is concluded as follows: first, the causes of SEA force measurement issues are modeled and analyzed in the viewpoint of deterministic and stochastic behavior. The results indicated that the errors characteristic of SEA force measurement is Gaussian; second, TFOB was developed to achieve precise force measurement with consideration of errors for motor-side position and spring deformation measurement. The verifications of TFOB-based force estimation performance showed that the optimal performance can be found at the specific frequency bandwidth of TFOB; third, TFOB-based force controller was designed to accurately control the output force of SEA. In addition, the tuning method for the controller was proposed by using the dynamics of the closed-loop SEA system and the investigated Gaussian behavior of the measurement error; and last, experiments have been performed to explore the error behavior, and to verify the precision of proposed TFOB-based force controller and the observer.

REFERENCES

- [1] C. Lee, S. Kwak, J. Kwak, and S. Oh, "Generalization of series elastic actuator configurations and dynamic behavior comparison," in *Actuators*, vol. 6, p. 26, MDPI, 2017.
- [2] S. Oh and K. Kong, "High-precision robust force control of a series elastic actuator," *IEEE/ASME Trans. Mechatronics*, vol. 22, pp. 71–80, Feb 2017.
- [3] N. G. Tsagarakis, D. G. Caldwell, F. Negrello, W. Choi, L. Baccelliere, V. Loc, J. Noorden, L. Muratore, A. Margan, A. Cardellino, *et al.*, "Walk-man: A high-performance humanoid platform for realistic environments," *Journal of Field Robotics*, vol. 34, no. 7, pp. 1225–1259, 2017.
- [4] K. Ohnishi, M. Shibata, and T. Murakami, "Motion control for advanced mechatronics," *IEEE/ASME Trans. Mechatronics*, vol. 1, pp. 56–67, March 1996.

- [5] F. Negrello, M. Catalano, M. Garabini, M. Poggiani, D. Caldwell, N. Tsagarakis, and A. Bicchi, "Design and characterization of a novel high-compliance spring for robots with soft joints," in *2017 IEEE International Conference on Advanced Intelligent Mechatronics (AIM)*, pp. 271–278, IEEE, 2017.
- [6] M. Wang, L. Sun, W. Yin, S. Dong, and J. Liu, "A novel sliding mode control for series elastic actuator torque tracking with an extended disturbance observer," in *2015 IEEE International Conference on Robotics and Biomimetics (ROBIO)*, pp. 2407–2412, IEEE, 2015.
- [7] W. Wang and S. Sugano, "Output torque regulation through series elastic actuation with torsion spring hysteresis," in *2014 IEEE International Conference on Robotics and Biomimetics (ROBIO)*, pp. 701–706, IEEE, 2014.
- [8] W. Choi, J. Won, J. Lee, and J. Park, "Low stiffness design and hysteresis compensation torque control of sea for active exercise rehabilitation robots," *Autonomous Robots*, vol. 41, no. 5, pp. 1221–1242, 2017.
- [9] M. Makarov, M. Grossard, P. Rodríguez-Ayerbe, and D. Dumur, "Modeling and preview H_∞ control design for motion control of elastic-joint robots with uncertainties," *Trans. Ind. Electron.*, vol. 63, no. 10, pp. 6429–6438, 2016.
- [10] J. Austin, A. Schepelmann, and H. Geyer, "Control and evaluation of series elastic actuators with nonlinear rubber springs," in *2015 IEEE/RSJ International Conference on Intelligent Robots and Systems (IROS)*, pp. 6563–6568, IEEE, 2015.
- [11] M. Ruderman, "Compensation of nonlinear torsion in flexible joint robots: Comparison of two approaches," *IEEE Trans. Ind. Electron.*, vol. 63, no. 9, pp. 5744–5751, 2016.
- [12] C. Lee, J. Lee, J. Malzahn, N. Tsagarakis, and S. Oh, "A two-staged residual for resilient external torque estimation with series elastic actuators," in *Humanoid Robotics (Humanoids), 2017 IEEE-RAS 17th International Conference on*, pp. 817–823, IEEE, 2017.
- [13] C. Mitsantisuk, M. Nandayapa, K. Ohishi, and S. Katsura, "Design for sensorless force control of flexible robot by using resonance ratio control based on coefficient diagram method," *automatika*, vol. 54, no. 1, pp. 62–73, 2013.
- [14] J. Lee, C. Lee, N. Tsagarakis, and S. Oh, "Residual-based external torque estimation in series elastic actuators over a wide stiffness range: Frequency domain approach," *IEEE Robotics and Automation Letters*, vol. 3, no. 3, pp. 1442–1449, 2018.
- [15] S. Yamada and H. Fujimoto, "Proposal of state-dependent minimum variance estimation of load-side external torque considering modeling and measurement errors," in *2018 IEEE 27th International Symposium on Industrial Electronics (ISIE)*, pp. 1–6, IEEE, 2018.
- [16] M. Ruderman and M. Iwasaki, "Sensorless torsion control of elastic-joint robots with hysteresis and friction," *IEEE Trans. Ind. Electron.*, vol. 63, no. 3, pp. 1889–1899, 2016.
- [17] S. Haddadin, A. De Luca, and A. Albu-Schäffer, "Robot collisions: A survey on detection, isolation, and identification," *IEEE Trans. Robot.*, vol. 33, no. 6, pp. 1292–1312, 2017.
- [18] T. Murakami, F. Yu, and K. Ohnishi, "Torque sensorless control in multidegree-of-freedom manipulator," *IEEE Trans. Ind. Electron.*, vol. 40, no. 2, pp. 259–265, 1993.
- [19] S. Oh, K. Kong, and Y. Hori, "Design and analysis of force-sensorless power-assist control," *IEEE Trans. Ind. Electron.*, vol. 61, no. 2, pp. 985–993, 2014.
- [20] C. Lee and S. Oh, "Integrated transmission force estimation method for series elastic actuators," in *2018 IEEE 15th International Workshop on Advanced Motion Control (AMC)*, pp. 681–686, March 2018.
- [21] N. Sivashankar and P. P. Khargonekar, "Induced norms for sampled-data systems," *Automatica*, vol. 28, no. 6, pp. 1267–1272, 1992.
- [22] C. Lee and S. Oh, "Configuration and performance analysis of a compact planetary geared elastic actuator," in *IECON 2016 - 42nd Annual Conference of the IEEE Industrial Electronics Society*, pp. 6391–6396, Oct 2016.